Materials Research Express

PAPER • **OPEN ACCESS**

Green gamma-irradiated chitosan/PVA–silver hydrogel for efficient methylene blue removal

To cite this article: Le Thi Thanh Nhi *et al* 2025 *Mater. Res. Express* **12** 125002

Materials Research Express

OPEN ACCESS

RECEIVED
1 August 2025

REVISED
11 November 2025

ACCEPTED FOR PUBLICATION
25 November 2025

PUBLISHED
3 December 2025

PAPER

Green gamma-irradiated chitosan/PVA–silver hydrogel for efficient methylene blue removal

Le Thi Thanh Nhi[1,2], **Pham Bao Ngoc**[3], **Tran Anh Tuan**[4], **Nguyen Thi Huynh Nga**[5], **Le Xuan Cuong**[3], **Thanh Hoa Tran**[6], **Trinh Ngoc Ai**[7], **Le Hoang Sinh**[6,*], **Dinh Quang Khieu**[8,*] and **Hiep Minh Nguyen**[3,*]

[1] Center for Advanced Chemistry, Institute of Research and Development, Duy Tan University, Danang City, Vietnam
[2] Faculty of Natural Sciences, Duy Tan University, Danang City, Vietnam
[3] Center of Radiation Technology and Biotechnology, Dalat Nuclear Research Institute, Lam-dong Province, Vietnam
[4] Department of Nuclear and Isotopic Techniques, Dalat Nuclear Research Institute, Lam-dong Province, Vietnam
[5] Department of Biology, Dalat University, Lam-dong Province, Vietnam
[6] The University of Danang- VN-UK Institute for Research and Executive Education, Danang City, Vietnam
[7] Department of Agriculture and Aquaculture, Tra Vinh University, Vinh Long Province, Vietnam
[8] University of Sciences, Hue University, Hue City, Vietnam
[*] Author to whom any correspondence should be addressed.

E-mail: sinh.le@vnuk.udn.vn, dqkhieu@hueuni.edu.vn and jackminhhiep@yahoo.com

Keywords: chitosan, dye treatment, gamma ray, polyvinyl alcohol, silver nanoparticles

Abstract

In the context of increasing water pollution by organic dyes, the development of environmentally friendly materials with effective treatment capabilities is urgently needed. This study aimed to synthesize a biodegradable nAg-CS/PVA hydrogel with high compatibility for dye adsorption applications. The dual gamma irradiation technique successfully synthesized nAg-CS/PVA hydrogel material from the immobilization of nAg-CS particles (particle size of 24.95 nm, a polydispersity index of 0.202, and zeta potential of + 20.7 mV) into the PVA polymer network. The formation of nAg-CS/PVA was confirmed by FTIR, DSC, and FESEM analyses, which showed that the strong interaction between the functional groups of chitosan and PVA, combined with the superior complexation ability of Ag, contributed to the enhancement of gelation and swelling properties. The synthesized hydrogel was applied to remove methylene blue (MB) with a maximum adsorption capacity (q_m) of 285.71 mg g^{-1} under optimal conditions (PVA solution 150 g l^{-1}, PVA:nAg-CS volume ratio of 8:2 and irradiation dose of 30 kGy). The neutron activation confirmed the successful immobilization of Ag nanoparticles, ensuring the minimal release of silver ions into the environment. These findings highlight the potential of nAg-CS/PVA hydrogel as an efficient and environmentally friendly material for the treatment of dye-contaminated wastewater.

1. Introduction

Environmental pollution from wastewater has long been a major concern, especially in developing countries. Conventional wastewater often contains heavy metals and numerous toxic organic compounds (OCs), such as dyes, antibiotic residues, and pesticides, which can cause ecological imbalances and pose serious public health risks. Over the past few decades, various physical, chemical, and biological methods, like coagulation flocculation [1], membrane filtration [2], adsorption on activated carbon [3], and biological degradation [4], have been used to remove dyes and toxic heavy metals. However, many of these methods face challenges such as high operational costs, incomplete degradation, secondary pollution, or limited reusability of the treatment media. Therefore, developing efficient, low-cost, environmentally friendly materials with strong adsorption capabilities is essential for sustainable wastewater treatment. In this context, the use of advanced hybrid or nanostructured materials has become a promising alternative, providing better surface activity, stability, and regeneration potential compared to traditional adsorbents.

In recent years, nano-sized metals and metal oxides have been widely applied in the purification of polluted water by photocatalyst [5], photoelectrocatalyst [6], membrane separation [7], ion exchange [8], coagulation [9], and adsorption [10]. Silver nanoparticles (nAg) have been investigated as potential adsorbents due to their outstanding properties, such as high surface area, high surface free energy, and abundance of active sites leading to suitable adsorbents [11]. The disadvantage of nAg is that they can limit the adsorption efficiency because they can agglomerate, oxidize, and be challenging to separate. In addition, the direct application of nAg in wastewater treatment can make it a water pollutant that causes adverse effects on aquatic organisms and human health [12, 13]. To overcome this shortcoming, scientists often combine nAg with stabilizers to control particle size, distribution, and shape [14, 15]. Recently, chitosan (CS), a natural nanopolymer containing D-glucosamine structural units with many functional groups such as $–NH_2$ and –OH on the CS surface with the advantage of being readily biodegradable and of natural origin [16], has been used to stabilize nAg by gamma-ray induced coupling method. The outstanding advantage of the process is that the reaction rate is fast and controllable, and the reaction takes place without the need for initiating chemicals, so the resulting product has high purity and does not contain toxic chemicals [17]. Besides CS, polyvinyl alcohol (PVA) with a high number of hydroxyl groups can form hydrogels with better mechanical and chemical stability; previous publications on the synthesis of hydrogels from PVA and chitosan by gamma radiation have also been reported with many advantages, such as large-scale production and green production without using any toxic chemicals [18, 19].

This study developed a new hydrogel with high treatment efficiency and biodegradability, aiming at its application in dye treatment in the textile industry. The double gamma irradiation method synthesized silver nanoparticle immobilized CS/PVA hydrogel (nAg-CS/PVA). The particle size and zeta potential of nAg-CS were analyzed, and the effects of PVA concentration, nAg-CS/PVA ratio, and irradiation dose on gelation rate, swelling degree, and dye treatment ability were evaluated. In addition, the study also considered the adsorption model (Langmuir, Freundlich), the influence of flow rate, initial concentration of Methylene blue (MB), as well as the amount of silver remaining after treatment, to optimize the performance and ensure environmental safety. MB is a cationic dye that has been widely used in textile, chemical, and pharmaceutical industries, and MB-containing wastewater will be characterized by a high flow rate, deep color, high concentration of OCs, and poor biodegradability [20]. Therefore, the adsorption capacity of the synthesized nAg-CS/PVA hydrogel for MB was investigated to demonstrate the potential application of this material in treating dye-contaminated wastewater.

2. Experimental procedure

2.1. Materials

Methylene blue (CAS 7220-79-3, 82%), chitosan (CAS 9012-76-4, $>$ 99%), silver nitrate (CAS 7761-88-8, 95%), sodium hydroxide (CAS 1310-73-2, 97%), Sodium metasilicate (CAS 6834-92-0, SiO_2 content 50%–53%), and ethylene glycol (CAS 107-21-1, $\geqslant$ 99%) were purchased from Sigma Aldrich (USA). Polyvinyl alcohol (CAS 9002-89-5, molecular weight: 60,000–125,000 g/mol) was supplied by HiMedia Laboratories (USA). Other chemicals were of analytical grade.

2.2. Synthesis of nAg-CS and nAg-CS/PVA solutions

The nAg-CS/PVA hydrogel was prepared by double gamma-irradiation method. In the first stage, a 10 g l^{-1} chitosan solution in 2 wt% acetic acid solution was neutralized with 5N NaOH solution to reach pH 5.5, and 20 ml of ethylene glycol and 5 g $NaSiO_3$ were added, respectively. Then, $AgNO_3$ was dissolved in the prepared chitosan solution to generate a 10 mM $AgNO_3$ solution. The solution was irradiated in a glass bottle using Co-60 gamma rays at a dose of 30 kGy. After irradiation, the samples were determined for particle size and zeta potential using a Zetasizer Nano ZS (Malvern, U.K.). In the second stage, nAg-CS/PVA nanomaterials were synthesized by free radical polymerization under the effect of gamma Co-60 radiation. Specifically, 50 g/l, 100 g l^{-1}, and 150 g l^{-1} PVA solutions in distilled water were stirred continuously at 250 rpm at 80 °C for 5 h. Then, brought to room temperature, the PVA solution was dispersed with nAg-CS according to the volume ratios of PVA:Ag-CS, respectively, 8:2, 5:5, and 3:7. The final mixtures were divided into PE bags and irradiated on a Gamma Chamber 5000 irradiator at doses of 30 kGy, 40 kGy, and 50 kGy before being dried at 40 °C to constant weight.

2.3. Characterization

The gel fraction was determined by soaking the dried samples in distilled water for 12 h at 80 °C, then rinsing them with hot water to remove the soluble fraction, and continuing to dry to constant weight at 40 °C. The

sample was then pulverized (⩽200 μm) and stored in a PE bag. Samples of purified material will be used for characterization.

The gel fraction was calculated using the following equation:

$$\text{Gel(wt.\%)} = \frac{W_d \times 100}{W_o} \quad (1)$$

where W_d and W_o are the dried mass of samples after and before extraction, respectively.

The swelling ratio was calculated using the following equation:

$$\text{Swelling ratio(g/g)} = \frac{W_s - W_o}{W_o} \quad (2)$$

where W_s and W_o are masses of swollen and dry samples, respectively.

The morphology of the fabricated materials was investigated using field emission scanning electron microscopy (FESEM; S-4800, Hitachi, Japan) and transmission electron microscopy (TEM; JEM-2100F, JEOL, Japan). Fourier transform infrared spectroscopy (FTIR; JASCO FT-IR 6300, Japan) determined the composition of functional groups on the material surface. The glass transition region of the material was analyzed using differential scanning calorimetry (DSC; DSC-60, Shimadzu, Japan). The mean particle size, polydispersity index (PDI), and zeta potential of nAg-CS were determined by dynamic light scattering (DLS) using a nano-ZS nano-size analyzer (Malvern, UK).

2.4. MB treatment

2.4.1. Adsorption capacity

In the adsorption experiment, the procedure was followed: 0.1 g of purified dry material was weighed and added to five conical flasks, each containing 100 ml of an MB solution with concentrations ranging from 50 to 500 mg l^{-1}. The mixtures were stirred at 250 rpm using a magnetic stirrer for 150 min. Subsequently, the solutions were filtered, and the remaining MB concentration was determined using UV–vis spectrophotometry (Shimadzu Model UV-1240, Japan) at an absorbance wavelength of 664 nm.

The kinetics of MB adsorption by the grafted material was determined by Langmuir and Freundlich isotherm model. The Langmuir isotherm model assumes that metal ion adsorption occurs on the surface of the monolayer adsorbent [21], where there is no interaction between the adsorbed ions, then Langmuir describes the interaction process between the adsorbent and the adsorbed metal ion by a linear equation of the form:

$$\frac{C_e}{q_e} = \frac{C_e}{q_m} + \frac{1}{q_m \cdot K_L} \quad (3)$$

Where q_e and q_m correspond to the adsorption capacity at equilibrium and maximum adsorption capacity, respectively (mg/g). K_L: Langmuir adsorption constant, C_e (mg/L): concentration of the solute in the liquid phase at equilibrium.

Freundlich isotherm model is another method used to describe multilayer adsorption and the heterogeneous surface of the adsorbent. The Freundlich equation in linear form is rewritten as [22]:

$$lnq_e = lnK_F + \frac{1}{n} lnC_e \quad (4)$$

Construct a graph of lnq_e dependent on lnC_e, from which, the adsorption constant K_F and exponent n can be determined in the Freundlich equation.

2.4.2. Dynamic efficiency of MB treatment

MB treatment efficiency of nAg-CS/PVA materials was determined by changing the flow rate and initial concentration of the MB solution. The experiment was carried out on a treatment column containing grafted material (plastic column, length 10 cm, diameter 1 cm). With the following steps: 1 g of the material was soaked in distilled water for 24 h to achieve optimum swelling, then packed the column. The 20, 50, and 100 mg l^{-1} MB solutions were passed through the column at a flow rate of 0.5, 1.5, and 2.5 ml min^{-1}. The solution is taken as a fractional volume after flowing through the column. Determine the concentration of MB remaining in the solution using the UV–vis method.

The adsorption efficiency was calculated according to the equation:

$$\text{Yield\%} = \frac{(C_0 - C_e)}{C_0} \cdot 100 \quad (5)$$

where C_0 and C_e are the initial and after-treatment MB concentrations, respectively.

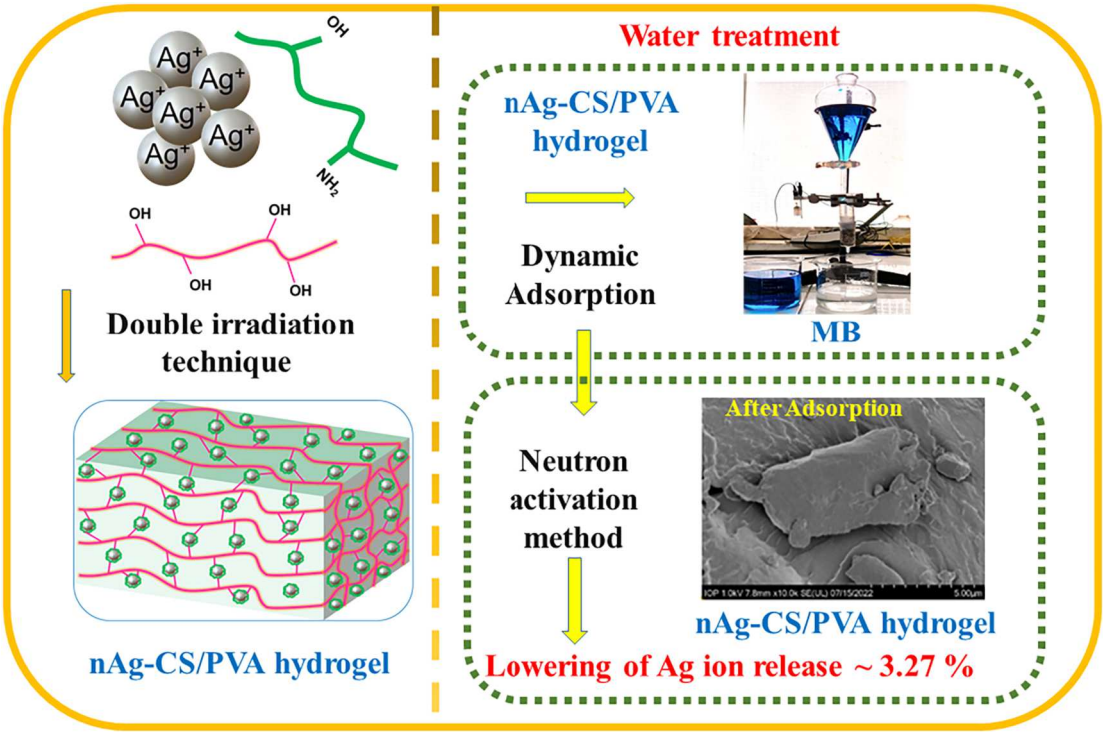

Scheme 1. Illustration of the synthetic process and MB adsorption.

2.4.3. Determination of silver content released into the water environment

The neutron activation method measured the total amount of silver in the nAg-CS/PVA hydrogel and the amount of silver released to the environment after treatment with MB solution (10000 ml, 50 mg/ml). The experiment was conducted on a neutron source at the rotating disk position of the nuclear reactor (the reactor has a nominal capacity of 500 kW). The turntable is located on the outer surface of the reflector with 40 sample cavities for long beams, and the sampling and placement time is about 30–60 seconds. Long projection is carried out on a turntable with a heat flux at the projection position of about 2.2 - 3.76 $\times$ 10^{12} n/cm^2/s. The probe used in the experiment is the HPGe GMX30190 ultra-pure semiconductor probe. Gamma Vision 6.0 software is used in spectrophotometric recording.

The process of synthesis and application for removal of MB is presented as Scheme 1.

3. Results and discussion

3.1. Formation of hydrogel nAg-CS/PVA

Figure 1 illustrates the synthesis of nAg-CS/PVA hydrogel by dual gamma irradiation. In the first step, gamma irradiation generates reactive species such as hydrated electrons and hydroxyl radicals that reduce Ag^+ ions to metallic Ag nanoparticles [23], forming silver nanoclusters, which further combine to form larger structures. They then bind to the functional groups, which contain amino and hydroxyl groups, serving as both a stabilizing agent by binding to the surface of the nanoparticles and a mild reducing agent, thus forming a well-dispersed nAg–CS complex [24, 25]. PVA is subjected to gamma irradiation, which induces the formation of macroradicals on its polymer chains. These radicals facilitate crosslinking between PVA and chitosan chains, entrapping the nAg–CS complexes within a three-dimensional polymeric matrix (nAg-CS/PVA hydrogel).

As shown in table 1, the nAg-CS nanoparticles had a narrow size distribution with a polydispersity index (PDI) of 0.202 and an average size of about 24.95 nm. In addition, the zeta potential of nAg-CS reached + 20.7 mV, indicating that the particle system was highly stable [16]. It can be explained by the strong electrostatic repulsion between positively charged particles, which prevents aggregation and maintains a stable nanosize.

The storage stability of nAg–CS was further assessed by monitoring particle size and zeta potential over a period of 0–8 weeks. Figure 2 illustrates the size distribution DLS of plain nanoparticles and nAg-CS on day 1 and day 14. As summarized in table 2, the particle size increased slightly from 25.37 nm to 40.04 nm. At the same time, the zeta potential remained above + 20 mV, suggesting that the nanoparticles retained good colloidal stability with only limited aggregation during storage. To further confirm the stability of the synthesized

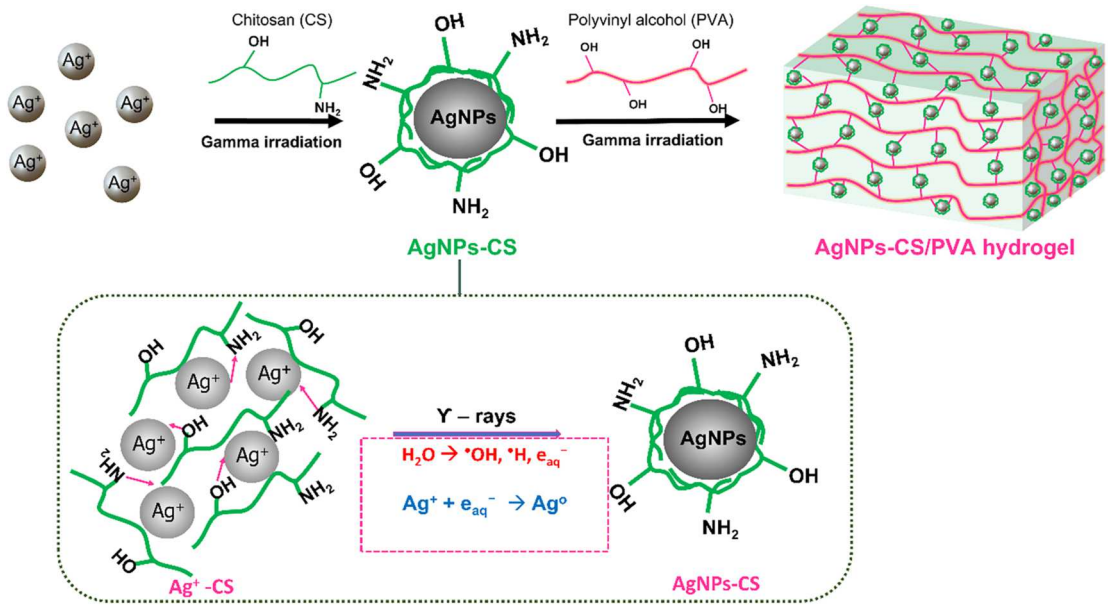

Figure 1. Formation of nAg–CS/PVA hydrogel via double gamma irradiation, involving AgNPs stabilization with chitosan followed by PVA–CS crosslinking into a 3D network.

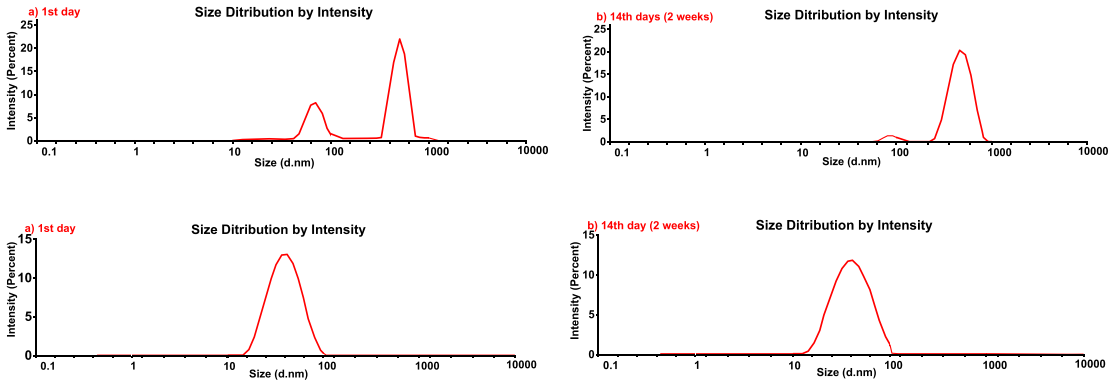

Figure 2. DLS size distribution of plain nanoparticles (upper) and nAg-CS (lower) on day 1 and day 14.

Table 1. Physical characteristics of nAg-CS (n = 3).

Mean particle size (nm)	Polydispersity index (PDI)	Zeta potential (mV)
24.95 ± 1.28	0.202 ± 0.011	+20.7 ± 0.4

nanoparticles, an agglomeration test was conducted to compare the storage stability of chitosan-functionalized nanoparticles with that of conventional nanoparticles.

The results in table 3 show that chitosan-functionalized nanoparticles exhibited a slight increase in particle size (from 26.16 to 28.92 nm). Over two weeks, they maintained a high positive zeta potential (+ 20.9 to + 20.5 mV), indicating moderate colloidal stability and limited agglomeration. In contrast, conventional nanoparticles showed a significant increase in size (from 569.2 to 910.8 nm) and a significant decrease in zeta potential (+4.7 to + 3.0 mV), indicating severe agglomeration and poor stability. These results clearly demonstrate that chitosan functionalization plays a crucial role in preventing aggregation and enhancing the stability of the nanoparticles, consistent with the positive zeta potential, which indicates strong electrostatic repulsion.

In addition, the high-resolution TEM image (figure 3(a) and inset) revealed that the nanoparticles were well-dispersed, spherical in shape, and had an average diameter of around 20 nm, which is consistent with the DLS measurements. Collectively, these findings confirm that nAg–CS was successfully synthesized via gamma

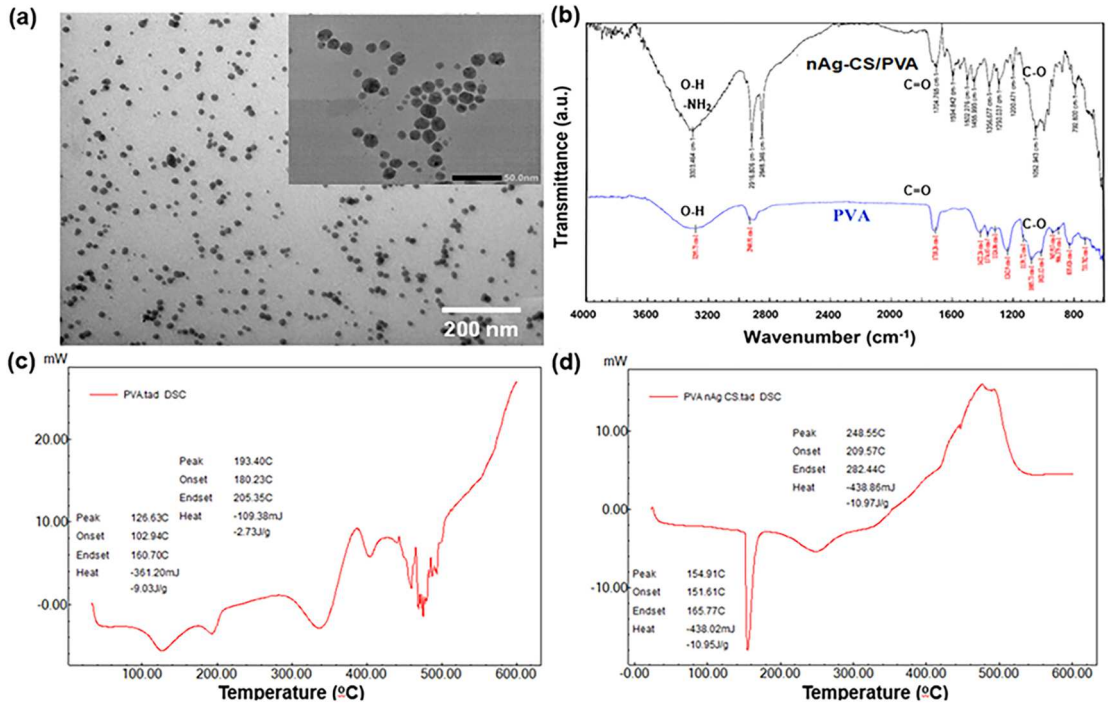

Figure 3. TEM image of nAg-CS (the inset presents the HRTEM of nAg-CS) (a); FTIR spectra of PVA and nAg-CS/PVA (b); DSC isotherm of PVA (c); and nAg-CS/PVA (d).

Table 2. Measuring the size of the nanoparticles after some storage time.

Times	Mean particle size (nm)	Zeta potential (mV)
0	25.37 ± 1.28	$+21.0 \pm 0.5$
1 week	26.23 ± 1.13	$+20.7 \pm 0.4$
2 weeks	27.54 ± 0.87	$+20.8 \pm 0.3$
4 weeks	32.37 ± 1.32	$+20.5 \pm 0.6$
8 weeks	40.04 ± 1.4	$+20.1 \pm 0.5$

irradiation, exhibiting good stability and dispersion, which are suitable for practical applications. Next, the characteristics of nAg-CS/PVA hydrogel were studied. Firstly, the FTIR spectrum of PVA (figure 3(**b**)) exhibited absorption peaks at 3295, 3424–1422, 1139, 1085, and 906–1085 cm^{-1}, corresponding to the oscillations of functional groups such as OH, $–CH_2$, C-C, C-O, and C–O, respectively [26, 27]. When comparing the FTIR spectra of PVA and nAg-CS/PVA hydrogel (figure 3(**b**)), changes in the shape and position of the $–NH_2$ and –OH vibrations around 3303 cm^{-1} can be observed, indicating the interaction between the hydroxyl groups of PVA with the hydroxyl or amine groups of chitosan during the formation of the hydrogel. In addition, the appearance of an absorption peak at 1704 cm^{-1} in the FTIR spectrum of nAg-CS/PVA hydrogel indicates the presence of carbonyl groups, suggesting that the gamma irradiation process may cause oxidation of the hydroxyl groups in PVA, chitosan or their hydrolysis products [28]. Furthermore, the interaction between Ag-NPs with electron-rich groups such as $–NH_2$ and –OH causes a slight shift of some spectral peaks and signal intensity changes. It confirms the presence of nAg in the hydrogel network, contributing to the material's structural properties and adsorption performance [29]. On the other hand, the DSC results showed that the melting temperature T_m and glass transition temperature T_g of PVA (figure 3(**c**)) and nAg-CS/PVA (figure 3(d)) had apparent changes. The glass transition temperature (T_g) of PVA was 126.6 °C, and the melting point (T_m) of PVA was 193.4 °C. Meanwhile, the glass transition temperature of the grafted nAg-CS/PVA material increased to 154.9 °C, indicating that hydrogen bonds were formed between the functional groups in the material structure of CS and PVA. Similarly, the significant increase in the material's melting point to 248.55°C indicated that the material's thermal stability was also significantly improved after the grafting process [30].

Table 3. Aggregation assay comparing the chitosan-functionalized nanoparticles vs. plain nanoparticles by irradiation method.

Samples	Times	Mean particle size (nm)	Zeta potential (mV)
Chitosan-functionalized nanoparticles	0	26.16 ± 1.11	+20.9 ± 0.4
	1 week	27.83 ± 1.28	+20.7 ± 0.5
	2 weeks	28.92 ± 1.25	+20.5 ± 0.4
Plain nanoparticles	0	569.2 ± 9.01	+4.7 ± 0.6
	1 week	769.6 ± 8.26	+3.16 ± 0.4
	2 weeks	910.8 ± 11.26	+3.02 ± 0.3

Table 4. Effects of PVA concentration, PVA/nAg-CS ratio and irradiation dose on gel content and swelling ratio of nAg-CS/PVA hydrogel material (n = 3).

PVA/nAg-CS volume ratio	Irradiation dose (kGy)	PVA concentration (g/L)					
		50		100		150	
		Gel content (wt%)	Swelling ratio (g/g)	Gel content (wt%)	Swelling ratio (g/g)	Gel content (wt%)	Swelling ratio (g/g)
8/2	30	90.42 ± 0.70	2.30 ± 0.10	88.49 ± 1.71	2.45 ± 0.20	87.49 ± 1.27	3.31 ± 0.19
	40	90.81 ± 1.64	1.92 ± 0.21	89.97 ± 0.92	2.29 ± 0.11	89.91 ± 1.72	3.15 ± 0.13
	50	91.99 ± 0.94	1.89 ± 0.16	91.43 ± 0.79	2.16 ± 0.12	90.33 ± 1.02	2.99 ± 0.21
	60	90.54 ± 1.22	1.76 ± 0.18	89.35 ± 0.75	2.08 ± 0.19	88.64 ± 0.48	2.78 ± 0.23
5/5	30	84.07 ± 1.10	1.84 ± 0.11	82.72 ± 0.97	2.15 ± 0.14	78.07 ± 1.06	2.79 ± 0.18
	40	84.95 ± 1.05	1.62 ± 0.22	83.57 ± 1.22	1.83 ± 0.13	80.43 ± 0.79	2.63 ± 0.19
	50	86.09 ± 0.69	1.47 ± 0.16	84.53 ± 1.23	1.78 ± 0.21	81.63 ± 1.54	2.48 ± 0.23
	60	85.21 ± 1.32	1.41 ± 0.20	83.31 ± 0.85	1.73 ± 0.17	80.02 ± 0.81	2.35 ± 0.18
3/7	30	72.54 ± 1.35	1.59 ± 0.23	69.18 ± 1.20	1.70 ± 0.18	67.07 ± 0.35	1.87 ± 0.11
	40	74.95 ± 1.56	1.29 ± 0.18	71.54 ± 1.50	1.34 ± 0.15	70.15 ± 1.15	1.66 ± 0.19
	50	79.61 ± 1.05	1.10 ± 0.16	74.83 ± 1.20	1.20 ± 0.17	72.11 ± 1.01	1.41 ± 0.12
	60	76.57 ± 0.77	1.06 ± 0.18	72.18 ± 1.33	1.03 ± 0.11	69.49 ± 0.66	1.24 ± 0.18

3.2. Effect of ratio of nAg-CS and PVA, and irradiation dose on gelation percent and swelling ratio of nAg-CS/PVA

As shown in table 4, when increasing the irradiation dose from 30 to 50 kGy, the gel content of the material gradually increased, reaching 92 wt% at the irradiation dose of 50 kGy (PVA solution 50 g/l, PVA/nAg-CS volume ratio of 8/2). When the radiation dose range was above 50 kGy, the level of gel formation was saturated and showed signs of decline. It can be explained that the higher the radiation dose, the greater the number of free radicals generated [31], and the greater the degree of crosslinking in the hydrogel, thus the greater the degree of gel formation [32]. However, at the radiation dose range above 50 kGy, radiation crosslinking and hydrogel cleavage co-occurred to different degrees, resulting in limited gel content and possible damage. Meanwhile, the swelling of the material decreased as the radiation dose increased. Notably, at the irradiation dose of 60 kGy, the swelling ratio of the material was 1.17–1.65 fold lower than the corresponding value at the irradiation dose of 30 kGy. It may be because when the radiation dose is high, the bond density in the polymer network bonding process increases, limiting water penetration into the void [33]. On the other hand, the results in table 4 also indicated that when the volume ratio of nAg-CS (silver concentration of 10 mM) in the mixture with PVA increased, the gel content of the material decreased, which can be explained by the accumulation of nanoparticles that interferes with functional interoperability group in the material and leads to lower gelation. In addition, the material's swelling rate depended on the PVA content presented in the formulation (including the increase in PVA concentration and the increase in the PVA ratio in the mixture of nAg-CS/PVA). Specifically, when the content of PVA was increased in the formulation, the swelling ratio significantly increased. Notably, the increase in PVA concentration from 50 g/l to 150 g l^{-1} resulted in a 1.15–1.60 fold increase in the swelling ratio of the material. The rate of increase can be explained by the increase in the content of PVA in the hydrogel material; the number of hydrophilic functional groups increases, contributing to the swelling ability of the hydrogel mixture materials. On the contrary, the swelling ratio of the hydrogel decreased as the amount of nAg-CS increased, which could be explained by the hydrophobicity of the silver nanoparticles

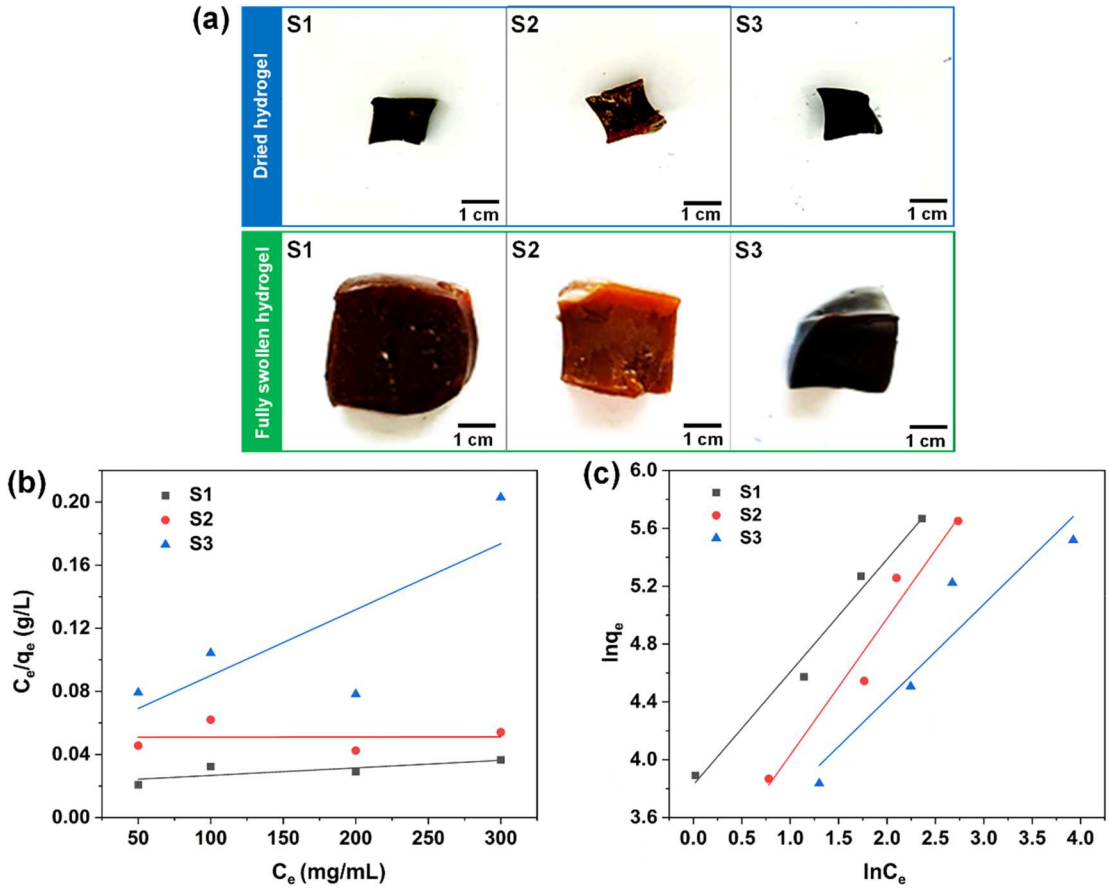

Figure 4. Images of gelation and swelling of S1, S2 and S3 samples (a); and their adsorption isotherm on Langmuir (b) and Freundlich (c) models for adsorption of MB.

Table 5. Adsorption isotherm parameters for MB by S1, S2 and S3.

Sample	Langmuir model			Freundlich model		
	R^2	q_m (mg/g)	K_L (L/mg)	R^2	n	K_F (mg/g)
S1	0.9994	285.71	0.294	0.6257	3.34	79.059
S2	0.9977	243.90	0.181	0.5748	3.05	62.809
S3	0.9953	222.22	0.149	0.6488	2.96	45.718

[34]. As shown in table 4, with increasing PVA content, the number of hydrophilic hydroxyl groups increased, increasing the polarity of the hydrogel, which reduced crosslinking and interfered with chain reactions in the material structure; thus, gelation was markedly reduced [35].

3.3. Adsorption capacity

Based on the results presented in section 3.2, the following experiments with three material samples with gel content above 86 wt%, namely S1 (volume ratio 8:2, PVA 150 g l^{-1}, 30 kGy), S2 (volume ratio 8:2, PVA 50 g/l, 30 kGy), and S3 (volume ratio 5:5, PVA 50 g/l, 50 kGy) for the highest, medium, and low swelling (figure 4(a)), were used to study the adsorption isotherms of the materials according to the Langmuir and Freudlich models. Figure 4(b)–c and table 5 show information related to the Langmuir and Freundlich adsorption isotherm models of the materials for MB.

The results show that the Langmuir model produced a higher linear correlation coefficient (R^2) than the Freundlich isotherm model, indicating that the Langmuir isotherm model better describes the adsorption of MB on the hydrogel material. It suggests that the adsorption of MB follows a monolayer and homogeneous process in which all adsorption sites on the adsorbent show the same affinity for the adsorbate [36]. Based on the Langmuir equation, the maximum adsorption capacities (q_m) of materials S1, S2, and S3 were 285.71 mg g^{-1}, 243.90 mg g^{-1}, and 222.22 mg g^{-1}, respectively. This difference may be due to the different

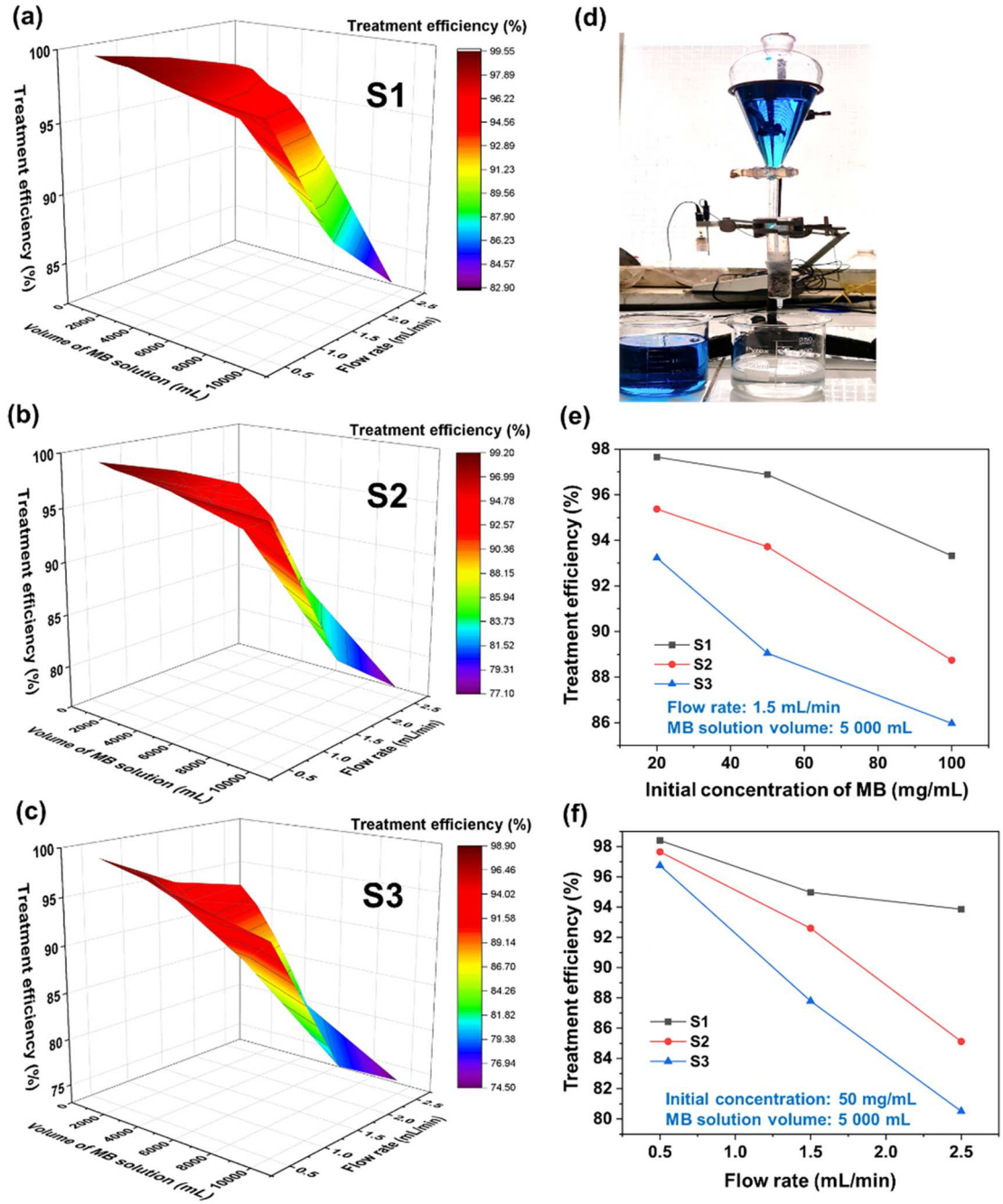

Figure 5. The effect of flow rate and volume of MB solutions on the treatment efficiency of S1 (a); S2 (b); and S3 (c); the dynamic adsorption experiment of MB (d); the effect of initial concentration of MB (e) and flow rate (f) on the treatment efficiency of S1, S2 and S3.

swelling degrees between the samples, in which S1 had a higher swelling degree than S2 and S3, 1.43 and 2 .25 times, respectively. Although these values represent the mass of the material, because of the small size of nAg, sample S3 with a higher silver content of 2440 mg/kg, exceeding samples S1 (947 mg/kg) and S2 (650 mg/kg) (table 5), still gave the lowest adsorption capacity. The following two reasons may explain that. First, the swelling ratio of S3 was approximately 2.25 and 1.56 times lower than that of S1 and S2 (table 2 and figure 4(a)), resulting in a smaller contact area between MB and the hydrogel material. Second, nAg could be oxidized from its elemental state (Ag^0) to silver ions (Ag^+) during repeated oxidation. This process degraded the catalytic capacity of nAg, resulting in a gradual decrease in the MB dye removal efficiency over time [37].

In general, the proposed mechanism for MB treatment with nAg-CS/PVA hydrogel is based on the good adsorption capacity of CS and PVA and the good catalytic efficiency of nAg. Chitosan acts as an immobilizer of nAg in the hydrogel material to avoid aggregation and as an adsorbent by electrostatic interaction with the cationic amino group (NH_3^+) of CS and hydrogen bonding to the hydroxyl group on the surface of both CS and PVA polymers [29]. Further, immobilizing nAg onto a carrier material enhances its effectiveness by providing

Table 6. Amount of silver content released into the water environment (n = 3).

Sample	$[Ag]^+_o$ (mg/kg)	$[Ag]^+$ after treatment (mg/kg)	Percentage of $[Ag]^+$ loss (%)
S1	947 ± 3.15	916 ± 4.20	3.27
S2	650 ± 2.90	570 ± 2.60	12.3
S3	2440 ± 2.24	2210 ± 2.72	9.42

more reactive centers and increasing absorption capacity. Therefore, immobilizing chitosan-stabilized nAg (nAg-CS) within a hydrogel matrix can significantly improve absorption capacity and treatment efficiency compared to using nAg alone. Furthermore, several studies have demonstrated the involvement of nAg in the mechanism of the rapid oxidation reaction. These studies indicate that the surface of nAg can adsorb nascent oxygen atoms or molecules capable of donating or accepting electrons. This electron transfer process facilitates the production of exceptionally reactive oxygen species responsible for oxidizing the dye compounds found in the surrounding environment [37, 38].

3.4. Investigation of MB treatment efficiency by dynamic adsorption method

Figure 5(**a**)–**c** provides an overview of the effects of MB solution volume and flow rate on the adsorption performance of three material samples, including S1, S2, and S3, with the treatment experiments set up as in figure 5(**d**). The results of all three samples showed a similar trend; when the flow rate was low, the contact time between MB and the adsorption center in the material was longer. This prolonged contact time enhanced the adsorption and led to a higher treatment efficiency. On the other hand, the results also showed that the treatment efficiency decreased as the MB solution volume increased due to the loss of nAg during the treatment process (table 6). The experimental conditions were set with a flow rate of 1.5 ml/min and a total MB solution volume of 5000 ml to investigate the effect of initial concentration on MB removal efficiency across three material samples (figure 5(**e**)). The results indicated that sample S1 exhibited the highest MB removal capacity among the three, with efficiency decreasing as the initial concentration increased. Specifically, at initial MB concentrations of 20 and 50 mg/l, sample S1 achieved removal efficiencies of 93.42% and 87.81%, respectively. However, when the concentration was increased to 100 mg l^{-1}, the efficiency dropped significantly to 82.78% under the same experimental conditions. This trend can be attributed to the adsorption mechanism occurring at active sites on the material surface. The adsorption sites remain largely unoccupied at lower concentrations, allowing for higher interaction and removal efficiency. In contrast, as concentration increases, the available adsorption sites become saturated, leading to a decline in treatment efficiency. As shown in figure 5(**f**) (derived from figure 5(**a**)–**c**), the MB removal efficiency of material S1 varied with flow rate. At a flow rate of 0.5 ml/min, S1 achieved a high efficiency of 97.45% for an MB solution (50 mg/ml). However, as the flow rate increased to 1.5 ml/min and 2.5 ml/min, the efficiency dropped to 87.81% and 82.92%, respectively, which indicates that higher flow rates reduce MB removal efficiency. The likely reason is that a lower flow rate allows for longer contact time between MB and the material, enhancing adsorption. Initially, abundant active sites on the material surface promote strong adsorption, but efficiency declines as these sites become saturated [39]. Furthermore, all adsorption sites are occupied at equilibrium, limiting further removal capacity [40, 41]. Additionally, figures 5a–c and 5f confirm that S1 consistently outperforms S2 and S3 at all flow rates, aligning with the maximum adsorption capacity (q_m) discussed in section 3.3.

3.5. Determination of Ag content released into the water environment

Considering the cytotoxicity of silver nanoparticles from previous studies [42], monitoring the release of Ag from hydrogels is crucial for evaluating their environmental safety. In this study, the Ag release test was performed to assess the stability and potential risk of secondary pollution during MB removal. The neutron activation method was used to measure the remaining silver content in the nAg-CS/PVA hydrogel samples after treating them with a 10000 ml MB solution. The results in table 6 demonstrated that sample S1 exhibited the lowest amount of silver lost to the environment (31 mg/kg), accounting for 3.27% of the total silver content in the material, despite having the highest swelling. Conversely, sample S3 experienced the highest silver loss (36.4% of the total silver content) while having the lowest swelling among the three samples. This discrepancy can be attributed to the higher or enough PVA present in sample S1 (150 g l^{-1} PVA solution and a PVA-to-nAg-CS volume ratio of 8:2), which facilitated the immobilization of nAg-CS particles within the hydrogel system. In contrast, the PVA content in sample S2 (50 g/l PVA solution and a PVA-to-nAg-CS volume ratio of 8:2) and sample S3 (50 g/l PVA solution and a PVA-to-nAg- CS volume ratio of 5:5) might have been insufficient compared to the total amount of nAg-CS present in the hydrogel. As a result, some nAg-CS particles were not

firmly bound to the hydrogel and could be quickly released into the environment. Furthermore, despite having the highest swelling, sample S1 exhibited approximately 97% retention of silver content after treating it with 10000 ml of the MB solution. It indicates the successful immobilization of nAg within the hydrogel material, minimizing silver loss and mitigating secondary pollution risks. The loss of silver content in the material following treatment with the MB solution can be explained by the diffusion of water into the hydrogel, facilitating reactions between silver atoms (Ag^o) and dissolved oxygen, forming a silver oxide (Ag_2O) layer. This silver oxide layer acts as a cluster containing silver ions, which remains within the system until further oxidation of Ag_2O occurs, producing Ag^+ ions that are eventually discharged into the external environment [43]. This low release level suggests that the prepared nAg-CS/PVA hydrogel exhibits high structural stability and minimal Ag leakage, thus reducing the cytotoxicity and enhancing its environmental relevance and safety for practical wastewater treatment applications. Additionally, the FESEM images of the nAg-CS/PVA sample after MB treatment (figure 3(**c**)–**d**) revealed that the material's surface did not exhibit significant differences compared to the untreated nAg-CS/PVA sample (figure 3(a)–b). This observation further supports that nAg-CS did not experience substantial losses when subjected to a treatment ratio of 1 g of nAg-CS/PVA material per 10000 ml of water.

4. Conclusions

The nAg-CS/PVA hydrogel materials were successfully synthesized by double irradiation technique, with the first step being gamma irradiation to obtain nAg-CS (particle size of 24.95 nm, a polydispersity index of 0.202, and zeta potential of +20.7 mV) and the second step being gamma irradiation to immobilize the nAg-CS particles onto the PVA circuits to form nAg-CS/PVA hydrogel. The formation of nAg-CS/PVA was confirmed by FTIR, DSC, and FE-SEM, which indicated the bonding between functional groups on the surfaces of chitosan and PVA polymer chains. This, combined with the strong complexing ability of Ag, led to the development of a hydrogel material with excellent gelation and swelling properties. The synthesized material was then applied for treating MB contained in the water. The results revealed that the MB adsorption process adhered to the Langmuir isotherm adsorption model with the maximum adsorption capacity (q_m) of 285.71 mg g^{-1} with the optimal conditions being sample parameters (150 g l^{-1} PVA solution and PVA:nAg-CS volume ratio of 8/2, 30 kGy). Moreover, the neutron activation method was employed to assess the remaining silver content in the material, which provided evidence of the successful immobilization of Ag nanoparticles within the nAg-CS/PVA hydrogel. The findings demonstrated that incorporating nAg into the hydrogel greatly enhanced the treatment efficiency while minimizing the release of Ag ions into the environment, thus reducing the potential for pollution. Consequently, these results highlight the promising potential of nAg-CS/PVA hydrogel materials for the treatment of environmental pollution, particularly in cases involving dye-contaminated wastewater. Notably, these materials offer the advantage of green synthesis, avoiding the creation of toxic pollutants, making them suitable for large-scale applications.

Conflict of interest statement

The authors report there are no competing interests to declare.

Data availability statement

All data that support the findings of this study are included within the article (and any supplementary files).

Author contributions

Le Thi Thanh Nhi
Conceptualization (equal), Data curation (equal), Formal analysis (equal), Investigation (equal)

Pham Bao Ngoc
Conceptualization (equal), Data curation (equal), Formal analysis (equal), Investigation (equal)

Tran Anh Tuan
Data curation (equal), Formal analysis (equal)

Nguyen Thi Huynh Nga
Data curation (equal), Formal analysis (equal)

Le Xuan Cuong
Data curation (equal), Formal analysis (equal)

Thanh Hoa Tran 0000-0002-5563-0670
Funding acquisition (equal), Methodology (equal)

Trinh Ngoc Ai
Funding acquisition (equal), Methodology (equal)

Le Hoang Sinh
Validation (equal), Writing – original draft (equal)

Dinh Quang Khieu 0000-0003-3473-6377
Visualization (equal), Writing – review & editing (equal)

Hiep Minh Nguyen 0000-0002-8441-5769
Validation (equal), Writing – original draft (equal)

References

[1] Wang K J and Wang P S 2025 Coagulation-flocculation process optimization for industrial wastewater treatment: a multi-objective computational solution *J. Water Process Eng.* **78** 108703
[2] Azmi L S, Jabit N 'A, Ismail S, Ku Ishak K E H and Abdullah T K 2025 Membrane filtration technologies for sustainable industrial wastewater treatment: a review of heavy metal removal *Desalin. Water Treat.* **323** 101321
[3] Shah H H, Amin M, Pepe F, Mancusi E and Fareed A G Overview of environmental and economic viability of activated carbons derived from waste biomass for adsorptive water treatment applications *Environ. Sci. Pollut. Res.* **32** 19084–109
[4] Nagraj, Chaurasia P K, Bharati S L, Sharma N, Kumar J and Sivalingam A M 2025 Degradation of dyes by fungi: An overview on recent updates *Microbe* **6** 100232
[5] Y. M A, A. M W, Parveen N, Al-Basri Y, Nivetha A and Ansari S A 2025 Advanced nanostructured oxide materials and composites for efficient heavy metal removal from water *Top Catal, Top. Catal.* (https://doi.org/10.1007/s11244-025-02199-5)
[6] Fareza A R, Nugroho F A A, Abdi F F and Fauzia V 2022 Nanoscale metal oxides-2D materials heterostructures for photoelectrochemical water splitting—a review *J. Mater. Chem. A* **10** 8656–86
[7] Bashambu L, Singh R and Verma J 2021 Metal/metal oxide nanocomposite membranes for water purification *Mater. Today Proc.* **44** 538–45
[8] Arora U and Tomar A 2025 Inorganic ion-exchange sorbents in the treatment of liquid radioactive wastes *in: Ion Exch. Process. Water Environ. Manag., Royal Society of Chemistry* ed A Somya and A Khan (Springer) 319–40
[9] Shabani N, Javadi A, Jafarizadeh-Malmiri H, Mirzaie H and Sadeghi J 2021 Potential Application of iron oxide nanoparticles synthesized by co-precipitation technology as a coagulant for water treatment in settling tanks *Mining, Metall. Explor.* **38** 269–76
[10] Dabas S 2025 Metal and metal oxide based nanoremediation: a sustainable alternative *Discov. Mater.* **5** 1–20
[11] Darweesh M A, Elgendy M Y, Ayad M I, Ahmed A M M, Kamel Elsayed N M and Hammad W A 2022 A unique, inexpensive, and abundantly available adsorbent: composite of synthesized silver nanoparticles (AgNPs) and banana leaves powder (BLP) *Heliyon* **8** e09279
[12] Jaswal T and Gupta J A review on the toxicity of silver nanoparticles on human health *Mater. Today Proc.* **81** 859–63
[13] Tortella G R, Rubilar O, Durán N, Diez M C, Martínez M, Parada J and Seabra A B 2020 Silver nanoparticles: toxicity in model organisms as an overview of its hazard for human health and the environment *J. Hazard. Mater.* **390** 121974
[14] Bharti S, Agnihotri S, Mukherji S and Mukherji S 2015 Effectiveness of immobilized silver nanoparticles in inactivation of pathogenic bacteria *Artic. J. Environ. Res. Dev.* **9** 849–56 https://researchgate.net/publication/278021309
[15] McGillicuddy E, Murray I, Kavanagh S, Morrison L, Fogarty A, Cormican M, Dockery P, Prendergast M, Rowan N and Morris D 2017 Silver nanoparticles in the environment: sources, detection and ecotoxicology *Sci. Total Environ.* **575** 231–46
[16] Mirajkar S, Rathod P, Pawar B, Penna S and Dalvi S 2021 γ-Irradiated chitosan mediates enhanced synthesis and antimicrobial properties of chitosan–silver (Ag) nanocomposites *ACS OMEGA* **6** 34812–22
[17] Wongpreecha J, Polpanich D, Suteewong T, Kaewsaneha C and Tangboriboonrat P 2018 One-pot, large-scale green synthesis of silver nanoparticles-chitosan with enhanced antibacterial activity and low cytotoxicity *Carbohydr. Polym.* **199** 641–8
[18] Linh L Q L D T P, Nghia N T, Vu N T and Ha T L T 2021 Synthesis of carboxymethyl chitosan-capped gold nanoparticles by gamma irradiation **2021** Article ID716550412
[19] Tran Vo T M, Piroonpan T, Preuksarattanawut C, Kobayashi T and Potiyaraj P 2022 Characterization of pH-responsive high molecular-weight chitosan/poly (vinyl alcohol) hydrogel prepared by gamma irradiation for localizing drug release *Bioresour. Bioprocess.* **9** 1–15
[20] Salehi G, Bagherzadeh M, Abazari R, Hajilo M and Taherinia D 2024 Visible light-driven photocatalytic degradation of methylene blue dye using a highly efficient Mg-Al LDH@g-C3N4@Ag3PO4 nanocomposite *ACS Omega* **9** 4581–93
[21] Lv G, Liu J, Xiong Z, Zhang Z and Guan Z 2016 Selectivity Adsorptive mechanism of different nitrophenols on UIO-66 and UIO-66-NH2in aqueous solution *J. Chem. Eng. Data* **61** 3868–76

[22] Yaffar D, Brenner J, Walker A P, Craig M E, Vaughan E, Marín-Spiotta E, Matos M, Rios S and Mayes M A 2025 The freundlich isotherm equation best represents phosphate sorption across soil orders and land use types in tropical soils of Puerto Rico *Biogeochemistry* **168** 1–15
[23] Beden S A J, Ati A A, Alimarah K A F, Saihood S K, Abdulnabi R K and Mejbel M K 2022 Green synthesis and characterization of silver nanoparticles / CM-chitosan-isopropanol by gamma irradiations Method *Rev. Des Compos. Des Mater. Av* **32** 173–80
[24] Elbarbary A M and El-Sawy N M 2017 Radiation synthesis and characterization of polyvinyl alcohol/chitosan/silver nanocomposite membranes: antimicrobial and blood compatibility studies *Polym. Bull.* **74** 195–212
[25] Naikwadi A T, Sharma B K, Bhatt K D and Mahanwar P A 2022 Gamma radiation processed polymeric materials for high performance applications: a review *Front. Chem.* **10** 1–15
[26] Betriani R, Sutarno S, Kartini I and Budiarta J 2023 Synthesis of zeolite/npk coated with Cu-alginate-PVA-glutaraldehyde as a slow-release fertilizer *Indones. J. Chem.* **23** 184–99
[27] Sun T, Zhan D, Wang X, Guo Q, Wu M, Shen P and Wu M 2024 Release and degradation mechanism of modified polyvinyl alcohol-based double-layer coated controlled-release phosphate fertilizer *Polymers* **16** 1–14
[28] Cruz-Segundo C M, Vasquez-Garcia S R, Flores-Ramirez N, Sanchez-Orozco R, Abdel-Gawwad H A, Santiago A A and Vargas J 2025 Development and characterization of electrospun chitosan-chitin-PVA nanofiber: exploring structural integrity, crystallinity, and thermal stability for advanced applications *J. Mater. Sci. Mater. Eng.* **20** 1–18
[29] Jasrotia S, Gupta S, Kudipady M L and Puttaiahgowda Y M 2025 Development and characterization of chitosan-PVA-tannic acid film for extended shelf life and safety of food products *ACS Omega* **10** 19361–78
[30] Suflet D M, Popescu I, Pelin I M, Ichim D L, Daraba O M, Constantin M and Fundueanu G 2021 Dual cross-linked chitosan/PVA hydrogels containing silver nanoparticles with antimicrobial properties *Pharmaceutics* **13** 1–18
[31] Jeong J-O, Park J-S, Kim Y-A, Yang S-J, Jeong S-I, Lee J-Y and Lim Y-M 2020 Gamma Ray-induced polymerization and cross-linking for optimization of PPy/PVP hydrogel as biomaterial *Polymers* **12** 111
[32] Suhail M, Wahab A, Wang G, An S, Kiran B, Jabeen N, Iqbal M Z, Kong X and Wu P C 2025 Preparation of natural polymer-based hydrogels for oral delivery of anti-malarial drug: *in vitro* and cytotoxicity evaluation *RSC Adv.* **15** 30378–86
[33] Sutradhar S C, Banik N, Islam M, Rahman Khan M M and Jeong J H 2024 Gamma radiation-induced synthesis of carboxymethyl cellulose-acrylic acid hydrogels for methylene blue dye removal *Gels* **10** 1–22
[34] Yang Y, Huang W, Liu P, An M, Liu Y and Zhou W 2025 Effect of hydrophilic and hydrophobic Ag NPs on absorption and silk properties of silkworms *ACS Sustain. Chem. Eng.* **13** 3718–27
[35] Popescu I, Constantin M, Pelin I M, Suflet D M, Ichim D L, Daraba O M and Fundueanu G 2022 Eco-friendly synthesized PVA/chitosan/oxalic acid nanocomposite hydrogels embedding silver nanoparticles as antibacterial materials *Gels* **8** 1–19
[36] Guo X, Zhao Z, Gao X, Dong Y, Fu H and Zhang X 2024 Study on the adsorption performance of modified high silica fly ash for methylene blue *RSC Adv.* **14** 21342–54
[37] Ghaedi M, Roosta M, Ghaedi A M, Ostovan A, Tyagi I, Agarwal S and Gupta V K 2018 Removal of methylene blue by silver nanoparticles loaded on activated carbon by an ultrasound-assisted device: optimization by experimental design methodology *Res. Chem. Intermed.* **44** 2929–50
[38] Mota D R, Martini W da S and Pellosi D S 2023 Influence of Ag size and shape in dye photodegradation using silver nanoparticle/ZnO nanohybrids and polychromatic light *Environ. Sci. Pollut. Res.* **30** 57667–82
[39] Marzbali M H and Esmaieli M 2017 Fixed bed adsorption of tetracycline on a mesoporous activated carbon: Experimental study and neuro-fuzzy modeling *J. Appl. Res. Technol.* **15** 454–63
[40] Moralez L, Nakasu P and Hallett J 2025 Preparation of hybrid β-chitosan - squid pen protein hydrogel beads by ionic liquid regeneration for adsorption of copper(ii) and zinc(ii) from wastewater *Soft Matter* **21** 2480–92
[41] Mohamad Sarbani N M, Hidayat E, Naito K, Aoyagi M and Harada H 2025 Enhanced stability and adsorption of cross-linked magnetite hydrogel beads via silica impregnation *J. Compos. Sci.* **9** 1–27
[42] Liao C, Li Y and Tjong S C 2019 Bactericidal and cytotoxic properties of silver nanoparticles *Int. J. Mol. Sci.* **20** 1–20
[43] He D, Garg S, Wang Z, Li L, Rong H, Ma X, Li G, An T and Waite T D 2019 Silver sulfide nanoparticles in aqueous environments: Formation, transformation and toxicity *Environ. Sci. Nano.* **6** 1674–87